13 A COMPARISON OF INFRARED GAS ANALYZERS ABOVE A SUBALPINE FOREST IN COMPLEX TERRAIN

Sean P. Burns[1,2*], Stefan Metzger[3], Peter D. Blanken[2], George Burba[4], Edward Swiatek[5], Jiahong Li[4], Benjamin Conrad[5], Hongyan Luo[3], and Jeff Taylor[3]

[1]National Center for Atmospheric Research (NCAR), Boulder, CO 80307
[2]Department of Geography, University of Colorado, Boulder, CO 80309
[3]National Ecological Observatory Network (NEON), Boulder, CO 80301
[4]LI-COR Biosciences, Lincoln, NE 68504
[5]Campbell Scientific, Inc., Logan, UT 84321

1. INTRODUCTION

Infrared gas analyzers (IRGAs) are a key component to the eddy covariance measurement of water vapor and carbon dioxide exchange between the surface and atmosphere (Aubinet et al., 2012). Historically, closed-path IRGAs designed for laboratory use (such as the LI-COR, model LI-6262) were used to measure H_2O and CO_2 fluxes in the atmosphere (e.g., McDermitt, 1997). These closed-path IRGAs worked best in climate-controlled conditions. In order to use them in the field these IRGAs were typically housed in temperature-controlled enclosures or buildings that were tens of meters away from the actual measurement location near the sonic anemometer. This necessitated the use of long tubing and high-power pumps to bring the air sample to the IRGA cell. Attenuation of H_2O and CO_2 fluctuations within the tubing was a persistent problem with such a setup, especially for H_2O (Massman, 1991; Lenschow and Raupach, 1991; Fratini et al., 2012). As an alternative, open-path IRGAs have frequently been utilized, but the key trade-offs with the open-path design are: (i) precipitation and dew affecting the measurements and creating data gaps, and (ii) the need to account for effects of air density changes on measured H_2O and CO_2 along the air sampling path (Leuning and Judd, 1996). Over the past five years a new type of closed-path IRGA has emerged. This newly-designed IRGA is weather-proof, compact, and low-maintenance. Furthermore, because of its small size, short intake tubing can be used, which places the sampling cell close to the sonic anemometer and reduces high frequency signal loss (e.g., Clement et al., 2009; Burba et al., 2010; Nakai et al., 2011; Burba et al., 2012; Novick et al., 2013). Two such IRGAs are the LI-COR LI-7200 and the Campbell Scientific EC155, which is part of the CPEC200 closed-path eddy covariance system.

*corresponding author address: Sean P. Burns, National Center for Atmospheric Research, P. O. Box 3000, Boulder, CO 80307-3000; *email*: sean@ucar.edu

At the University of Colorado (CU) AmeriFlux tower near Niwot Ridge, Colorado, a LI-6262 IRGA has been deployed since 1998 to measure ecosystem fluxes with 10 m long Synflex 0.625 cm composite tubing transporting the air sample from the 21.5 measurement level to the LI-6262 located about halfway up the tower (Monson et al., 2002). The LI-6262 has been out of production for over 10 years and requires factory maintenance about every two years. To take advantage of the new design features mentioned above and reduce instrument maintenance costs, we wanted to upgrade the LI-6262 to a newer model IRGA. However, one difficulty with changing the analyzer in the middle of such a long-term measurement program is that the upgraded sensor can potentially bias conclusions about the environmental phenomena being measured. Therefore, we deemed it crucial to better understand any instrument-dependent measurement differences over the full range of environmental conditions experienced at this specific site. Consequently, starting in summer 2013, a LI-7200 (along with an open-path LI-7500) were deployed at 21.5 m on the AmeriFlux tower. In Fall 2013, a EC155/CPEC200 was added so that a side-by-side comparison between all four IRGAs was possible (Fig. 1). The preliminary results presented in our study use data collected during March, 2014 to compare: the CO_2 and H_2O mean and variance measured by each IRGA, the vertical wind statistics from three side-by-side sonic anemometers, as well as the corresponding spectra and cospectra from these sensors.

2. COMPARISON DETAILS

2.1 Niwot Ridge subalpine forest site description

Our study uses data from the Niwot Ridge Subalpine Forest AmeriFlux site (site US-NR1, more information available on-line at http://ameriflux.lbl.gov) located in the Rocky Mountains about 8 km east of the Continental Divide.

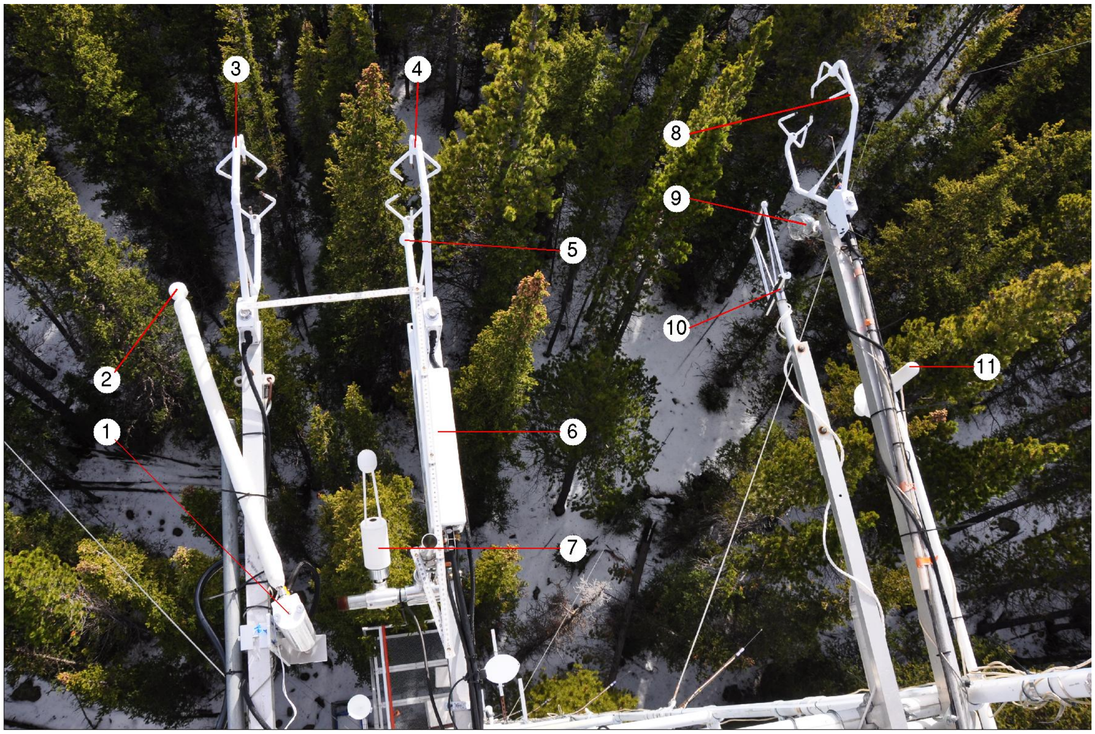

Figure 1: Photograph from 24 October 2013 looking down at the instrumentation deployed at 21.5 m on the University of Colorado AmeriFlux Tower. Various numbered instruments are described in Table 1. The booms for each CSAT3 are pointed in a nominal direction of 203 degrees from true north. For further deployment details see http://uquell.colorado.edu/calendar/.

The site is located on the side of an ancient moraine with rocky (granite) mineral soil and a shallow layer ($\approx$ 10 cm) of organic material (Scott-Denton et al., 2003). The forest near the tower is around 110 years old, and primarily composed of subalpine fir (*Abies lasiocarpa* var. *bifolia*), lodgepole pine (*Pinus contorta*), and Englemann spruce (*Picea engelmannii*). The tree density near the AmeriFlux Tower is around 4,000 trees ha^{-1} with a leaf area index (LAI) of 3.8-4.2 m^{2}m^{-2} and tree heights of 12–13 m (Turnipseed et al., 2002; Monson et al., 2010). The long-term mean annual precipitation is around 800 mm with about 40% of the total from warm-season rain (Hu et al., 2010). From November–January, the weather at the site is characterized by cold mid-continental conditions and strong downslope winds are frequent (Burns et al., 2012). Snow typically covers the ground from mid-November until late May. In March, the ecosystem is typically a weak source of CO_2 to the atmosphere due to microbial activity under the snowpack coupled with a senescent forest (Monson et al., 2006; Bowling et al., 2009). Because the forest is not taking up CO_2, there is no transpiration, and latent heat flux is small relative to that of the growing season. Such conditions present a challenge for eddy covariance instrumentation, because the ecosystem fluxes are relatively small and environmental changes such as air temperature and wind speed are large (Fig. 2).

2.2 Measurements on the AmeriFlux tower

2.2.1 Nomenclature and units

The mole fraction of CO_2 relative to dry air (or mixing ratio) will be designated as χ_c (units: μmol CO_2 per mole of dry air) which we will refer to as "dry mole fraction" in our discussion (e.g., Kowalski and Serrano-Ortiz, 2007). The ecosystem flux of CO_2 is designated F_c with units of μmol m^{-2} s^{-1}. For CO_2, the World Meteorological Organization (WMO) maintains the WMO-scale which is a set of calibration gases that are used world-wide as a standard against which all CO_2 measurements should be related to (Zhao and Tans, 2006). For water vapor, χ_h is the variable used for the mixing ratio of H_2O (units: mmol H_2O per mole of dry air) and latent heat flux (LE, units: W m^{-2}) for the ecosystem flux of water vapor. Positive fluxes indicate transport of the scalar away from the surface and into the atmosphere.

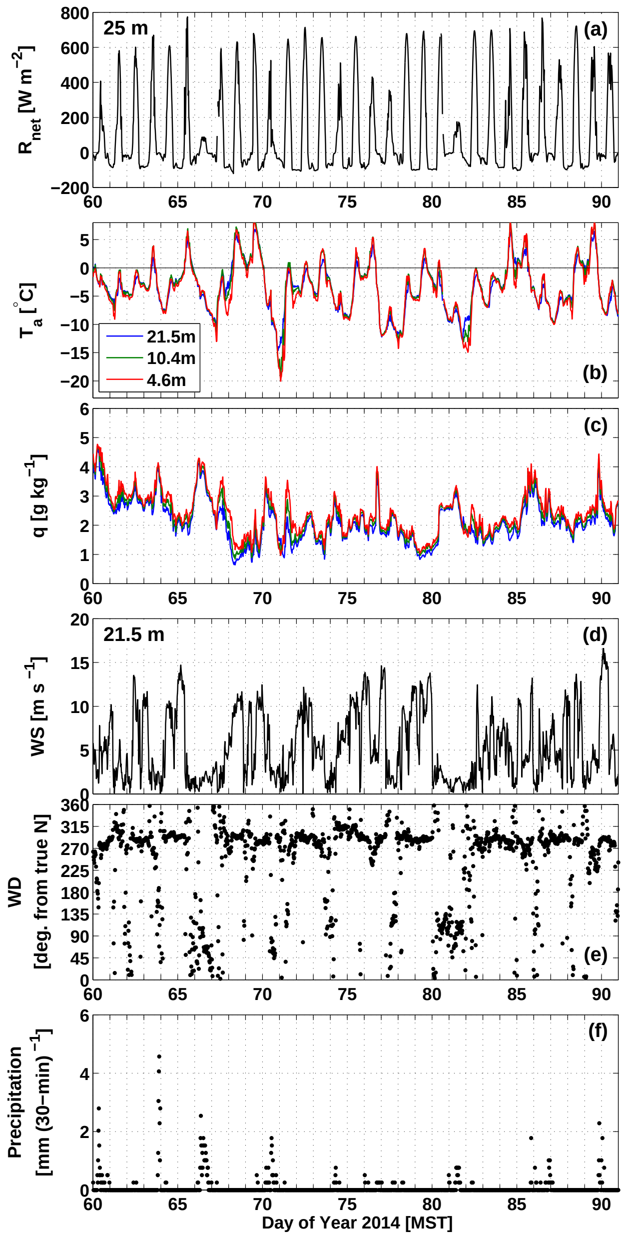

Figure 2: Time series of (a) 25-m net radiation R_{net}, (b) air temperature T_a, (c) specific humidity q, (d) 21.5-m wind speed WS, (e) 21.5-m wind direction WD, and (f) precipitation at the AmeriFlux tower during March, 2014. T_a and q are calculated from the slow-response Vaisala HMP35-D sensor while WS and WD are from the CU CSAT3 (Table 1).

Unless noted otherwise, all statistics and spectral estimates are made over a 30-min period. A summary of the instruments and nomenclature used in our study are provided in Fig. 1 and Table 1.

For density-based measurements with an open-path IRGA, the vertical CO_2 flux can be calculated by taking into account the WPL terms (Webb et al., 1980; Fuehrer and Friehe, 2002),

$$\underbrace{F_c}_{\substack{\textbf{CO}_2\\\textbf{Flux}}} = \underbrace{\overline{w'\rho_c'}}_{\textbf{Covariance}} + \underbrace{\mu\frac{\overline{\rho_c}}{\overline{\rho_a}}\overline{w'\rho_v'}}_{\substack{\textbf{Water Vapor}\\\textbf{Term}}} + \underbrace{(1+\mu\sigma)\frac{\overline{\rho_c}}{\overline{T}}\overline{w'T'}}_{\substack{\textbf{Temperature}\\\textbf{Term}}}, \tag{1}$$

where ρ_c, ρ_v, and ρ_a are the density of CO_2, water vapor, and dry air [units: g m^{-3}], respectively. The vertical wind component is w, μ is the ratio of the molar mass of dry air to the molar mass of water, and σ is the ratio of mean water vapor density to the mean dry air density. An overbar signifies the mean value and the prime are fluctuations over the 30-min period. In Eq.1, we have not included any higher-order or pressure terms which are discussed elsewhere (e.g., Fuehrer and Friehe, 2002; Burba et al., 2012). The temperature T would be T_a for an open-path IRGA, whereas for a closed-path IRGA it would be temperature fluctuations within the sample cell. For the purpose of our comparison, it is useful to realize that there are two WPL terms: one related to the water vapor fluctuations (second term on right-hand side of Eq.1) and one related to air temperature fluctuations (third term on right-hand side of Eq.1). In a closed-path system, the WPL temperature term is typically accounted for by either a fast-response temperature measurement of the air sample or through heat transfer within the air sample to remove any temperature fluctuations (e.g., Burba et al., 2012). In this case, the CO_2 dry mole fraction can be calculated directly using the ideal gas law and measured cell temperature and pressure. The WPL water vapor term can be avoided by using coincident high-rate water vapor measurements within the sample cell to directly convert ρ_c to χ_c using the dilution properties of water vapor on the CO_2 measurement, though phase differences between the CO_2 and H_2O should be considered (e.g., Ibrom et al., 2007). For the LI-6262 system, in addition to the long inlet tubing, a 1-m long coil of copper tubing inside the LI-6262 enclosure is designed to remove any residual temperature fluctuations within the air sample (Monson et al., 2002).

2.2.2 Wind measurements

Each IRGA in our study was paired with a Campbell Scientific CSAT3 sonic anemometer to measure the turbulent wind fluctuations. The "EOL" CSAT3 was paired with the LI-7200 inlet and the "CU" CSAT3 was paired with the LI-6262 inlet (Fig. 1). The EOL and CU CSAT3 have a 2 measurement sample pipeline delay which has been taken into account in the data analysis (Campbell Scientific, 2010). These sonic data were collected using the Synchronous Device for Measurements (SDM)

Table 1: Instrumentation and measurements from the Niwot Ridge AmeriFlux tower in March, 2014. All sensors are at a nominal height of 21.5 m above the ground.

Label from Fig. 1	Sensor type[a]	Manufacturer[b] make/model	Serial No. and CSAT3 firmware	Measured Variables[c]	Data Sample Rate samples/s	Deployment Dates[d]	Additional Comments
①, inlet ②, body	CP IRGA	LI-COR, LI-7200	72H-0479	χ_c, χ_h	20	2 Nov 2013–present	On 2 Nov 2013, sn 72H-0192 was replaced with sn 72H-0479
③	3D Sonic	CSI, CSAT3 (“EOL” CSAT3)	0254 (ver4)	u, v, w, T_s	10	27 Jul 2012–present	
④	3D Sonic	CSI, CPEC200/ CSAT3A	2047 (ver4)	u, v, w, T_s	10	8 Oct 2013–present	
⑤, inlet ⑥, body	CP IRGA	CSI, CPEC200/ EC155	1073	χ_c, χ_h	10	7 Jan 2014–present	On 7 Jan 2014, sn 1012 was replaced with sn 1073
⑦	OP IRGA	LI-COR, LI-7500	75H-0084	ρ_c, ρ_v	10	8 Oct 2013–16 May 2014	
⑧	3D Sonic	CSI, CSAT3 (“CU” CSAT3)	0198 (ver4)	u, v, w, T_s	10	28 Sep 2010–present	
⑨, inlet	CP IRGA	LI-COR, LI-6262	IRG3-0638	χ_c, χ_h	10	7 May 2013–present	Factory service and recalibration in May, 2013
⑩	Krypton Hygrometer	CSI, KH2O	1249	ρ_v	10	23 Jul 2013–present	Factory service and recalibration in July, 2013
⑪	Platinum resistance, capacative humidity	Vaisala, HMP35-D	N.A.	T_a, RH	1	N.A.	slow-response platinum resistance thermometer in a mechanically-aspirated housing

[a] CP and OP IRGA refers to closed-path and open-path infrared gas analyzers, respectively. 3D Sonic refers to a three dimensional sonic anemometer-thermometer.

[b] LI-COR: LI-COR Biosciences, Lincoln, NE 68504; CSI: Campbell Scientific, Inc., Logan, UT 84321.

[c] These are: CO_2 dry air mole fraction χ_c, H_2O dry air mole fraction χ_h, CO_2 density ρ_c, H_2O density ρ_v, air temperature T_a, relative humidity RH, sonic temperature T_s, and the planar-fit streamwise u, crossstream v, and vertical w wind components.

[d] Deployment dates refer to this particular instrument at this particular location.

communication protocol developed by Campbell Scientific. The EOL CSAT3 also output an analog voltage into the LI-7550 Analyzer Interface Unit which serves as the electronic control and network interface for the LI-7200. This allowed for the CSAT3 wind data to become part of the LI-7200 high-rate data archive. However, the analog CSAT3 sonic data has a reduced resolution compared to the SDM data. For example, the vertical wind analog output has a range of $\pm 8.192\,\mathrm{m\,s^{-1}}$ and resolution of $0.004\,\mathrm{m\,s^{-1}}$ whereas the SDM vertical wind has an autorange scale that goes up to $\pm 65.535\,\mathrm{m\,s^{-1}}$ and resolution between 0.00025 and $0.002\,\mathrm{m\,s^{-1}}$) (Campbell Scientific, 2010). Because we have simultaneously collected the SDM and analog CSAT3 wind data we can evaluate the effect of the reduced measurement range and resolution on the ecosystem fluxes.

The CPEC200 system includes a CSAT3A sonic anemometer which uses the same support frame and transducers as the CSAT3, but includes the EC100 electronics module to integrate the CSAT3A with the EC155 (Campbell Scientific, 2013a). For our comparison project, the CPEC200 bandwidth setting was at 5-Hz and therefore the introduced delay in winds from the CSAT3A and CO_2/H_2O from the EC155 are all 0.8 sec (8 samples). Unless stated otherwise, any comments provided about the CSAT3 equally apply to the CSAT3A. All of the sonic anemometers are using version 4 of the CSAT3 firmware.

Prior to the flux calculations, the measured wind components were transformed using the planar-fit method (e.g., Wilczak et al., 2001) which projects the measured wind vector into streamwise u, crossstream v, and vertical w wind components relative to the plane formed by the long-term averaged u and v wind components. The wind components in the sonic-coordinate reference frame will be designated as u_1, v_1, and w_1. The vertical wind fluctuations from each CSAT3 are compared with each other to ensure that any differences in the calculated fluxes were not due to sonic anemometer differences. The winds at the site are typically either downslope ($WD \approx 270°$) or upslope ($WD \approx 90°$) such that winds coming from behind the CSAT3s and through the tower infrastructure are rare (Fig. 2d).

2.2.3 Carbon dioxide measurements

The characteristics of each CO_2-measurement system used in our study are described in Tables 1 and 2. Every four hours, the LI-6262 sampled a CO_2-free gas (Ultra High Purity (UHP) N_2) and a so-called span gas, which is air with a fixed CO_2 dry mole fraction close to that of the atmosphere (typically around $400\,\mu\text{mol}\,\text{mol}^{-1}$). The UHP N_2 was used to determine the instrument offset while the span gas was used to determine any additional adjustment to the gain from the factory-determined calibration of the LI-6262. Prior to 2011, the dry mole fraction of the calibration span gas was determined using a second IRGA (LI-COR, model LI-6251) and a WMO-referenced calibration gas in a trailer near the tower (Monson et al., 2002). However, for the past several years, CO_2 measured by a tunable diode laser (described below) has been used for an *in situ* determination of the calibration span gas dry mole fraction. By using a CO_2-free gas and a single span gas, the LI-6262 can be considered a very precise instrument, but not necessarily highly accurate relative to the WMO CO_2-scale which requires taking into account the non-linearity of the IRGA response (Trivett and Köhler, 1999; Welles and McDermitt, 2005; Burns et al., 2009; Fratini et al., 2014).

Carbon dioxide dry mole fraction has also been measured on the AmeriFlux tower with a tunable diode laser (TDL) absorption spectrometer (Campbell Scientific, model TGA100A) since the summer of 2003 (Bowling et al., 2005; Schaeffer et al., 2008). The TDL CO_2 dry mole fraction is calibrated with four WMO-scale-related calibration gases and has a reproducibility estimated to be about $0.2\,\mu\text{mol mol}^{-1}$ relative to the WMO scale (Schaeffer et al., 2008). For our study, the TDL inlet at 21.5 m AGL was used to evaluate the mean CO_2 measured by the three IRGAs as well as an *in situ* determination of the LI-6262 calibration span gas dry mole fraction.

The LI-7200 and CPEC200 were generally operated according to the manufacturers recommendations and were setup with the characteristics shown in Table 2. Both systems used the factory-calibration and were operated without any span or zero calibration gases. More details on the internal digital signal filtering and instrument frequency response for the CPEC200 can be found in Sargent (2012). It has recently been observed that the inlet assembly design and rain-cup volume are important limiting factors in the IRGA frequency response (Metzger et al., 2014). As part of our comparison project, the LI-7200 used a non-standard heated inlet assembly (designed in cooperation with NEON) and raised the temperature of the incoming air sample by about 5–7°C. Power to the heated inlet was controlled with an adjustable DC power supply that was set to ≈ 3.8 W for the IRGA comparison. The results related to the frequency response due to a heated inlet and rain-cup design are summarized in a companion study by Metzger et al. (2014). The heated inlet for the EC155 is a part of the CPEC200 system and can provide anywhere from 0–0.7 W of power (for the IRGA comparison it was set to 0.7 W).

2.2.4 Water vapor measurements

Each IRGA compared in our study measures water vapor along with CO_2. The measurement of both H_2O and CO_2 in the same closed-path sample cell allows for the dilution correction to be applied directly to the high-rate data samples which precludes use of the WPL water vapor term as discussed in Sect. 2.2.1.

On the AmeriFlux tower, the LI-6262 measures the water vapor portion of the latent heat flux, but the primary sensor used for water vapor fluctuations has usually been the krypton hygrometer. The krypton hygrometer is preferred to avoid the long (10 m) tubing used by the LI-6262 which is especially problematic for water vapor because it interacts more with the inner wall of the tubing than CO_2 which attenuates the high-frequency water vapor fluctuations. There are several time periods when the krypton hygrometer was not available and the LI-6262 has been used for gap-filling during these times (with an empirical correction applied to try and compensate for the high-frequency signal loss). Water vapor measured by the LI-6262 uses the same UHP N_2 to determine the offset in the calibration. However, because there is no simple way to apply a span for H_2O (as is used for CO_2), a slow-response Vaisala HMP temperature/humidity sensor located near the LI-6262 inlet has been used to "span" the water vapor measurement.

2.3 Flux processing and calculations

In recent years there has been an active interest in ecosystem flux calculations using the eddy covariance technique which has led to several textbooks (e.g., Aubinet et al., 2012; Burba, 2013) as well as software development, such as EddyPro©.

For the initial calculation of the eddy covariance fluxes, we used a simple technique for all three IRGAs. Even though there is a long list of possible corrections to

Table 2: Details of the CO_2-measuring instruments used in our study.

	LI-6262[a]	LI-7200	EC155	TGA100A[a]
Manufacturer Manual	LI-COR (1996)	LI-COR (2013)	Campbell Scientific (2013b)	Campbell Scientific (2004)
Alternate Reference	Monson et al. (2002)	Burba et al. (2010)	Novick et al. (2013)	Schaeffer et al. (2008)
Calibration Gases [μmol mol^{-1}]	0 and 395.4	None	None	Four WMO-based Calibration Gases
Calibration Frequency	every 4 hrs	N.A.	N.A.	Hourly
Pump/Blower Characteristics	Rotary Vane (GAST, (model 1531-107B-G557X)	Blower (LI-7200-101 Flow Module)	Diaphragm (CPEC200 Pump Module)	Unknown
Inlet Distance from Sonic Path	≈15 cm	22.2[b] cm	15.6 cm	N.A.
Intake Tubing Characteristics	Bare Tubing, (Synflex, Type 1300)	Heated/Insulated Stainless Steel	Heated/Insulated Stainless Steel	Bare Tubing (Synflex, Type 1300)
Heated Inlet Assembly	No	Yes (≈ 3.8 W)	Yes (0.7 W)	No
Inlet Filter	2-μm (NuPro)	2-μm (Swagelok)	20-μm (steel disk)	1-μm (Nuclepore)
Tubing Length	≈1000 cm	80 cm	58.4 cm	≈2000 cm
Tubing Inner DIA	0.4318 cm ID	0.533 cm ID	0.267 cm ID	0.4318 cm ID
Cell Volume	11.9 cm^3	16 cm^3	5.9 cm^3	N.A.
Tubing Volume	146.44 cm^3	17.85 cm^3	3.27 cm^3	N.A.
Nominal Flow Rate	8.5 lpm	16 lpm	7 lpm	N.A.
Sample Travel Time[c]	1.12 s	0.127 s	0.079 s	N.A.
Sample Rate of Archived Data	10 Hz	20 Hz	10 Hz	1 Hz (multiple levels)
Bandwidth Setting	None	10 Hz	5 Hz	None
Time Keeping[d]	NTP (russter2)	PTP (russter2)	GPS	Unknown
Data System	CR23X + NIDAS[e]	LI-7550 + USB	EC100 + CR3000	CR3000
Variables Ingested by NIDAS data system[f]	All	CO_2	CO_2	None

[a] Both the LI-6262 and TGA100A are no longer in production

[b] On 12 Nov 2013, the LI-7200 inlet was moved from approximately 29.7 cm to 22.2 cm from the EOL CSAT3 sonic path

[c] The time for the air sample to travel from the inlet through the sample cell is calculated based on the volumetric flow rate U_{flow} and total displacement volume of the travel path V_{tot}, following, $t_{flush} = V_{tot} / U_{flow}$

[d] Time keeping refers to how the data system clock is synced to the true time; "russter2" is the on-site linux-based PC that runs NIDAS, archives the AmeriFlux tower data, and is an NTP/PTP server

[e] The NCAR In-Situ Data Acquisition Software (NIDAS) is open-source software developed at the NCAR Earth Observing Laboratory (EOL) and used for data acquisition from a large variety of atmospheric research instrumentation on aircraft and surface platforms (Maclean and Webster, 2012)

[f] To ensure time stamps are correct between the various instruments, an analog CO_2 voltage output from both the LI-7200 and EC155 were collected at 10-Hz by the NIDAS data system

apply (see examples listed in Mauder et al. (2008)), one of the underlying assumptions of our comparison is that the vertical turbulent fluxes sampled by each IRGA were similar. Therefore, our goal is not to measure the true ecosystem flux (which would require storage and horizontal transport estimations). Instead, we intend to establish what differs in the vertical turbulent fluxes measured by each instrument. For this reason we omit any spectral corrections for high-frequency signal loss. Rather, high-frequency signal loss is something we can evaluate by comparing the measurements from each instrument. For simplicity, only two transformations were applied to the high-rate data prior to calculating the fluxes: first, the planar-fit was applied to the wind components; second, each scalar was adjusted by a constant time-lag. The time-lag for the scalars were estimated from the time shift that resulted in the maximum correlation between the vertical wind fluctuations and the fluctuations of each scalar (either H_2O or CO_2). A rough estimate of the time lag can also be determined from the time it takes to flush the inlet tubing and sampling cell which are shown for each IRGA in Table 2. Future analysis will take into account more complicated corrections such as humidity-dependent lags which have been shown to be important, especially for water vapor fluxes (Fratini et al., 2012).

2.4 Additional information about data collection

In order to perform a proper instrument comparison of high-frequency data, time-keeping is an important consideration (Table 2). The data system at the AmeriFlux tower uses a set of six Campbell Scientific CR23X data loggers coupled with the NCAR In-Situ Data Acquisition Software (NIDAS) developed at the NCAR Earth Observing Laboratory (EOL) to collect and archive the high-rate data (Maclean and Webster, 2012). Each CR23X streams serial data at a rate of either 1-Hz or 10-Hz to a laptop at the base of the tower. Even though the individual CR23X clocks may drift over time, NIDAS time-tags the incoming serial data samples as they are ingested by the laptop using network time protocol (NTP) to ensure that the time-stamps are accurate. The LI-7200 uses precision time protocol (PTP) to ensure accurate time-keeping and 20-Hz raw data were stored on the internal USB thumb drive. A linux-based PC located in a trailer about 500 m from the tower (connected to the tower by a fiber optic cable) acted as the NTP/PTP server for the tower as well where the raw NIDAS data files were collected and archived. The CPEC200 system was equipped with a GPS for precise time-keeping and scan interval regulation. The CPEC200 10-Hz raw data were stored locally on a Campbell Scientific CR3000 data logger.

As a way to check for any potential differences among the clocks managing each of the three IRGAs, an analog CO_2 voltage from the LI-7200 and EC155 were ingested by the tower data system. This provided an easy way to check that the IRGAs were both working properly during the project as well as creating the potential for post-processing quality-control analysis of any time-stamp differences between the various data sets.

3. RESULTS

The comparisons presented herein often involve differences in measurements between two instruments. As part of our analysis, we will display these differences using box plots (e.g., box-and-whisker plots) which displays the data in quartiles (Hoaglin et al., 1983). The inner box is the inner quartile range (IQR) which is where 50% of the data exist while the "whiskers" and outliers (shown as individual points) are where the other 50% exist. The outliers are defined as points that are beyond 1.5 times the IQR from the inner quartiles. The IQR is a robust estimate of the variability in the difference because data in the highest and lowest quartiles do not affect it. We use the IQR extensively in our comparisons.

3.1 Comparison of CSAT3 vertical wind statistics

Because the sonic anemometers were leveled according to gravity and the tower is situated on a 6% slope, a strong horizontal wind (i.e., wind speed $WS > 10$ m s^{-1}) produced a vertical wind component in sonic coordinates with mean values around 2 m s^{-1} (Fig. 3a). The mean differences in w_1 among the three CSAT3s were on the order of 0.2–0.4 m s^{-1} with an IQR of the difference that was around 0.3–0.5 m s^{-1} as shown by the difference box plots in Fig. 3a.

After applying the planar-fit, the mean vertical wind in the rotated coordinate system for all three CSAT3s becomes smaller than ± 0.2 m s^{-1} and the IQR of the differences among the CSATs is reduced by an order of magnitude (Fig 4a). In addition, the planar-fit reduced the difference of the standard deviation of the vertical wind between CSAT3s from an IQR of around 0.1 m s^{-1} (Fig. 3b) to less than 0.05 m s^{-1} (Fig 4b).

3.2 IRGA characteristics

The cell temperatures of each IRGA were affected by changes in air temperature. Because the LI-6262 cell is deep within the electronics and it was housed in an enclosure halfway up the tower, the LI-6262 cell temperature was typically about 12-17 °C higher than the air temperature (Fig. 5a). The LI-7200 inlet was heated such that the air entering the cell was about 5–7 °C above T_a. While inside the LI-7200 cell, the air sample was cooled by

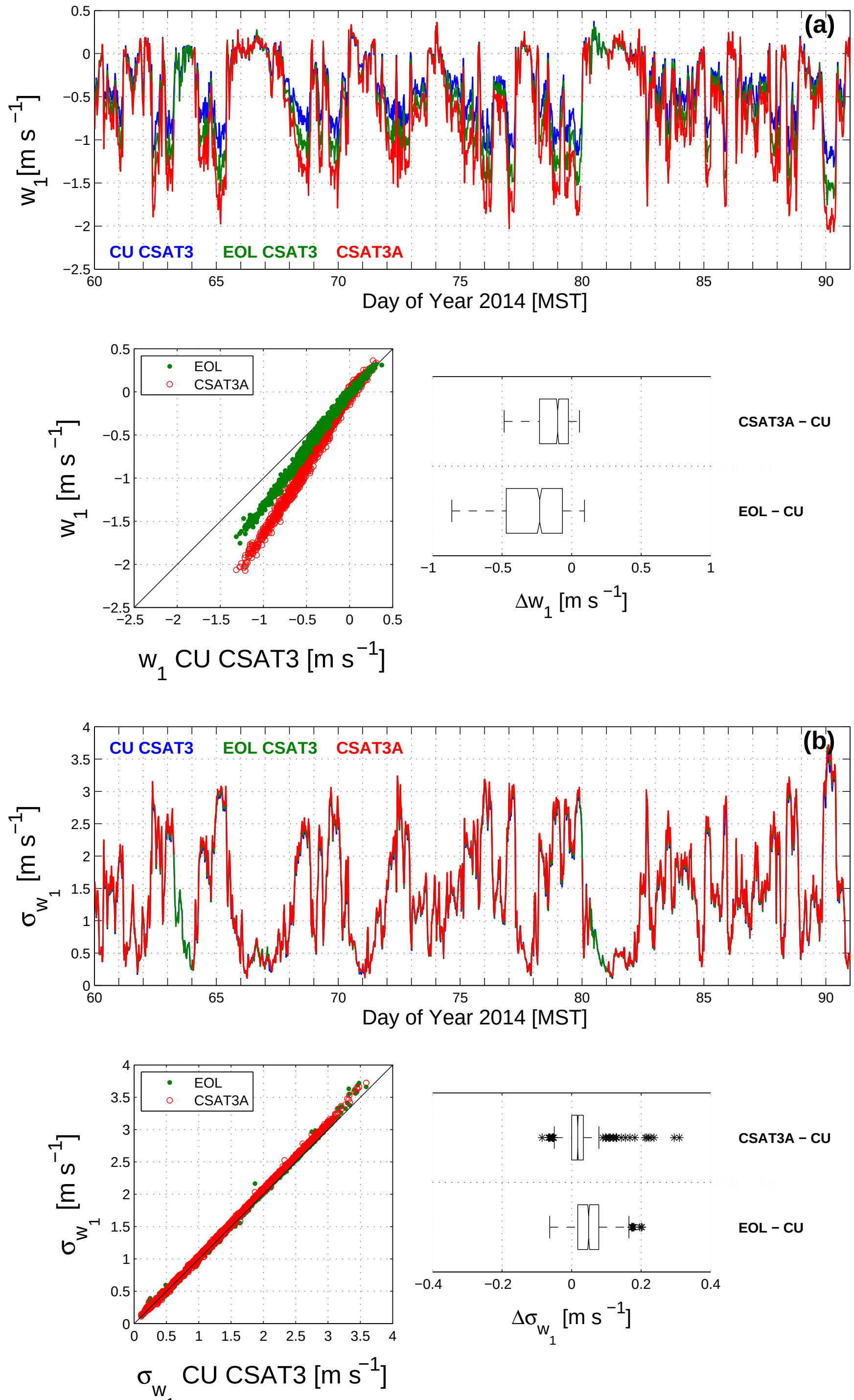

Figure 3: Time series, scatter plots, and box plots of (a) 30-min mean vertical wind in sonic coordinates w_1, and (b) standard deviation of vertical in sonic coordinates σ_{w_1} from March, 2014. In the scatter plots, the CU CSAT3 is on the abscissa. In the box plots, the differences relative to the CU CSAT3 are shown. The box plot shows the differences in quartiles where the inner box is the middle 50% of the data called the inner quartile range (IQR). In the box plot, outliers are shown as single points.

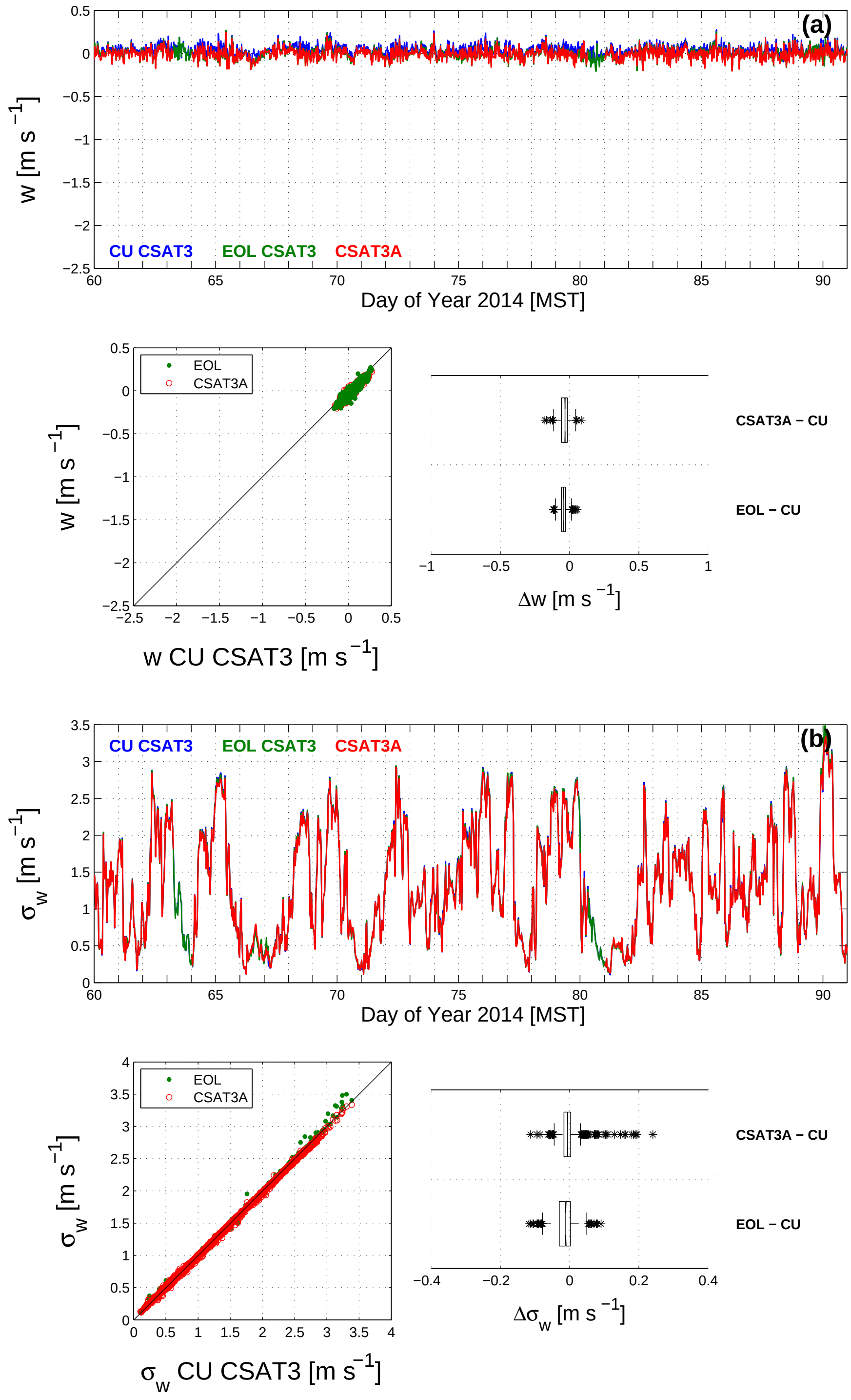

Figure 4: As in Fig. 3, except the vertical wind is shown in planar coordinates (i.e., w and σ_w).

2–5 °C suggesting that the overall cell temperature was anywhere from 1–5 °C above T_a. The CPEC200 sample intake was also heated and the cell temperature was around 1-2 °C above T_a.

To overcome the viscous and turbulent drag resistance due to the long tubing and resistance due to the inlet filter, the LI-6262 required a strong pump which created a pressure drop on the order of 13 kPa to maintain the flow rate at around 9 lpm (Fig. 5b, c). The cell pressure deficit and flow rates for the LI-7200 and EC155 were around

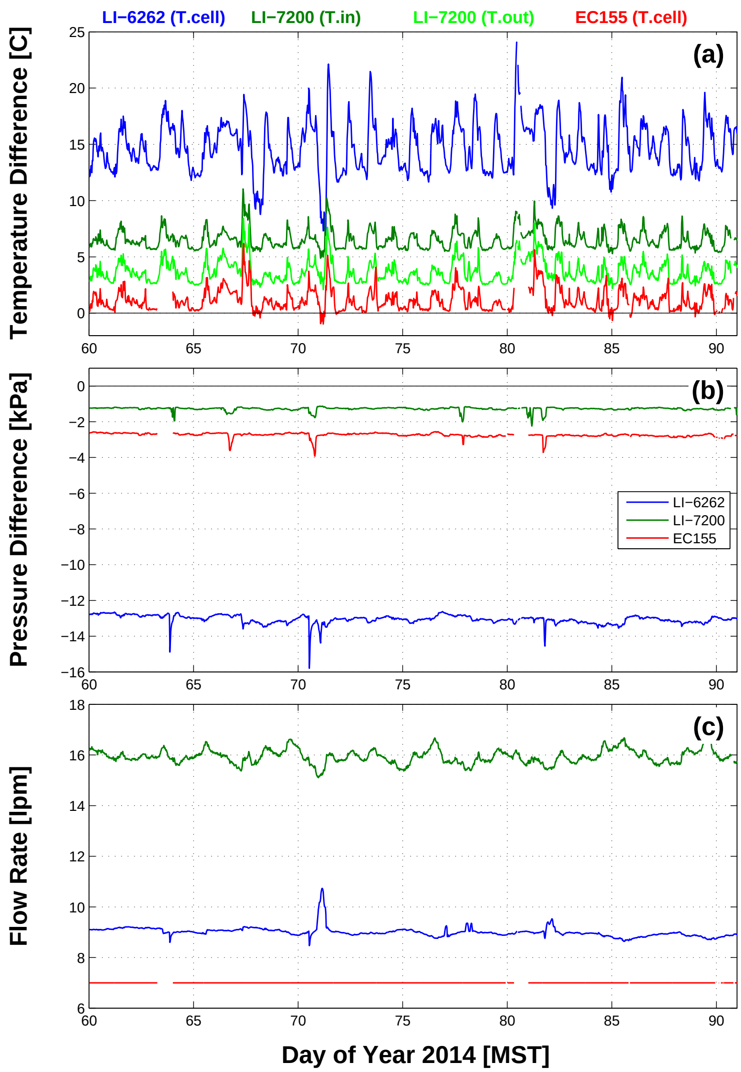

Figure 5: Time series of (a) temperature within the instruments relative to air temperature, (b) cell pressure relative to atmospheric pressure, and (c) the flow rate within each IRGA. The legend above (a) shows which temperature sensor is used and the legend in (b) also applies to (c).

1 kPa and 16 lpm, and 3 kPa and 7 lpm, respectively.

3.3 Comparison of mean and variance of CO_2 and H_2O from IRGAs

If we examine the time series for CO_2 dry mole fraction, it is immediately obvious that the EC155 χ_c had variations on the order of 15 μmol mol^{-1} that are not observed by any of the other three CO_2 instruments (Fig. 6a). Because the LI-6262 span gas dry mole fraction was based on the TGA measurements, these two systems were within 1 μmol mol^{-1} of each other and the IQR of the difference was less than 0.5 μmol mol^{-1} as shown by the box plot in Fig. 6a. Relative to the LI-6262, the LI-7200 had a bias of about 8.5 μmol mol^{-1}, but the IQR was less than 1 μmol mol^{-1} which suggests this difference was due to a calibration offset, not an error in the instrument gain (Table 3).

For the standard deviation of χ_c, the LI-7200 and EC155 both measured slightly smaller values than the LI-6262, however, similar to mean χ_c, there were larger variations in the EC155 – LI-6262 difference (IQR = 0.107 μmol mol^{-1}, Table 3) than the LI-7200 – LI-6262 difference which had an IQR of 0.022 μmol mol^{-1} (Fig. 6b).

For water vapor, the three IRGAs agreed much better

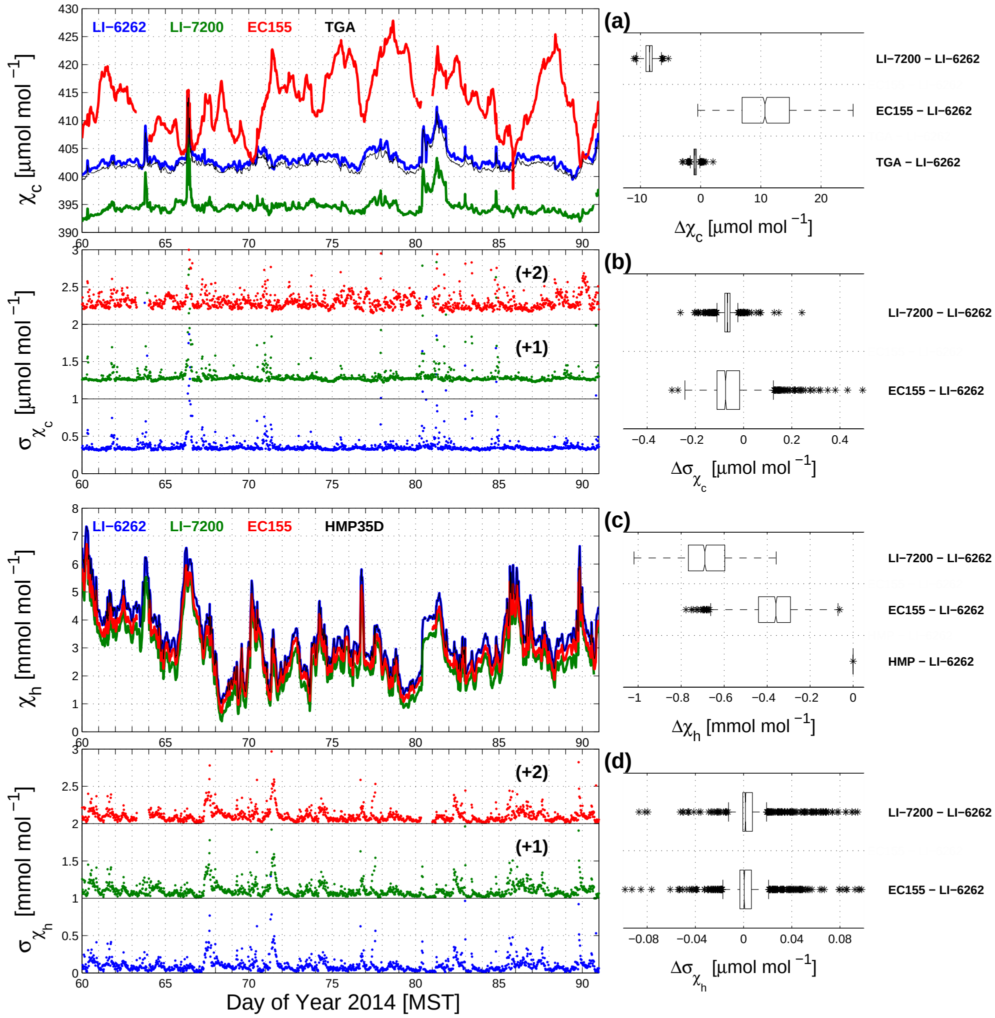

Figure 6: Comparison of the 30-min mean and standard deviation (σ) of (upper panels) CO_2 dry mole fraction χ_c and (lower panels) H_2O dry mole fraction χ_h from the LI-6262, LI-7200, and EC155 from March, 2014. Left panels are time series while the right columns are box plots of the differences. For mean χ_c, the University of Utah TGA100A 21.5m χ_c is the black line. For χ_h, the slow-response HMP T/RH χ_h is the black line. The TGA100A and HMP data are used for calibration of the LI-6262 χ_c and χ_h (see text for details).

with each other. We found that the LI-7200 mean χ_h was around 0.7 mmol mol^{-1} smaller than the LI-6262, while the EC155 χ_h was about 0.3 mmol mol^{-1} smaller than the LI-6262 (Fig. 6c). The IQR of the differences for the instrument pairs were both around 0.16 mmol mol^{-1} (Table 3). For the standard deviation of χ_h, the LI-7200 and EC155 were also both slightly larger than the LI-6262 and the box plots of the differences were similar (Fig. 6d).

3.4 Calculated time lags

As mentioned in Sect. 2.3, time lags were estimated based on the maximum correlation between the vertical wind and the scalar. Typically the vertical wind precedes the scalar because of the time it takes the air sample to travel from the inlet location to the measurement cell. The lag results for CO_2 and H_2O for each of the three IRGAs are shown in Fig. 7 where a negative value indicates how many seconds the scalar was behind the vertical wind. Because of the long tubing, the LI-6262 had the largest lags, with an average lag time of 2.6 s for CO_2 and 3.0 s for H_2O. When the humidity was high and/or precipitation occurred there were large changes to the lag for H_2O. For example, precipitation occurred on days 67, 70, and 86 (Fig. 2f) and all three IRGAs show that the lag for H_2O increased dramatically on those dates (Fig. 7).

We also roughly estimated the flushing time based on

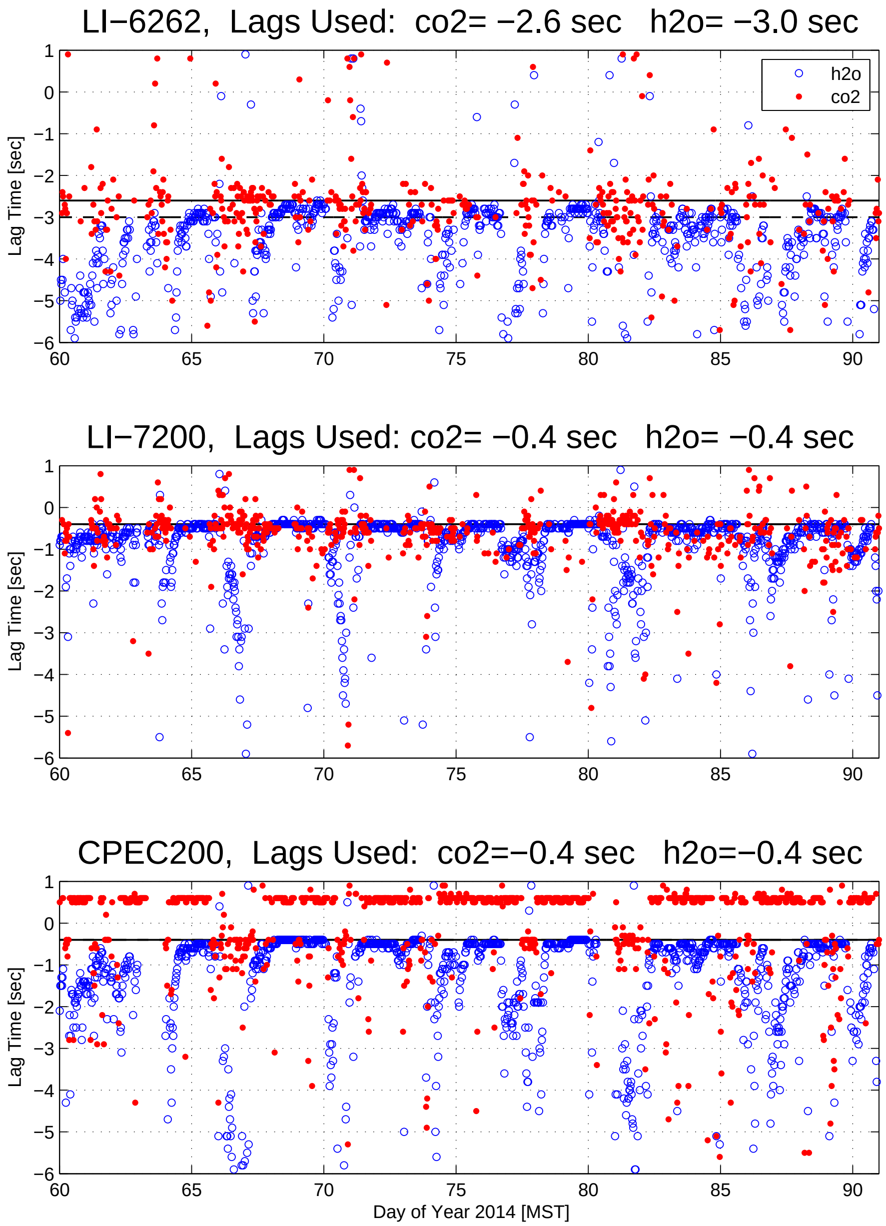

Figure 7: Estimated lag times between vertical wind and scalars from the LI-6262/CU CSAT3, LI-7200/EOL CSAT3, and EC155/CSAT3A. Only time periods with a p-value (e.g., Devore, 1987) smaller than 10^{-15} are shown. The text above each panel and horizontal black lines show the lag times used in the flux calculations.

the volumetric flow rate and total air volume of the sample cell and tubing (Table 2). In general these travel times were about 50–75% shorter than those estimated from the correlation technique. This rough estimate does not take into account that the air travel time depends on several additional items such as: the state of the airflow (turbulent versus laminar), filters, bends and turns in the airstream path, as well as the separation distance between the air inlet and the CSAT3 measurement volume.

One unusual result from the lag calculation was that CO_2 for the EC155 was found to lead the vertical wind (except during periods of precipitation) as shown in the bottom panel of Fig. 7. Though the scalar might lead the vertical wind for certain conditions, it is unlikely that this would be a typical state. One would also not expect the lag for CO_2 to be opposite in sign to the H_2O lag. Therefore, for the data processing, the EC155 lag for H_2O was used for CO_2 as shown in Fig. 7. Future analysis will take into account the effect of humidity on the scalar lag times.

Table 3: Summary of the IRGA comparison from March, 2014. The 30-min mean and standard deviation (σ) are both compared. The second and third columns are the mean and standard deviation of the LI-6262 measurements. The comparison results are presented as a mean $\pm$ the standard deviations of the difference relative to the LI-6262. Where appropriate, the inner quartile range (IQR) of the difference is shown in parentheses below the other statistics (see text for discussion of the IQR).

Variable (units)	LI-6262 Value		LI-7200 − LI-6262		EC155 − LI-6262	
	Mean	σ	Mean	σ	Mean	σ
χ_c	403.13 ± 1.76	0.41 ± 1.46	−8.54 ± 0.81	−0.07 ± 0.06	10.87 ± 5.54	−0.04 ± 0.31
[μmol mol^{-1}]			(1.04)	(0.022)	(7.87)	(0.107)
χ_h	3.40 ± 1.15	0.10 ± 0.10	−0.69 ± 0.12	0.005 ± 0.038	−0.37 ± 0.12	0.003 ± 0.035
[mmol mol^{-1}]			(0.17)	(0.014)	(0.16)	(0.021)
F_c	0.53 ± 0.39	N.A.	−0.04 ± 0.32	N.A.	−0.93 ± 1.06	N.A.
[μmol m^{-2} s^{-1}]			(0.62)		(1.36)	
LE	24.08 ± 31.68	N.A.	6.11 ± 16.59	N.A.	4.17 ± 13.56	N.A.
[W m^{-2}]			(28.12)		(20.47)	

3.5 Comparison of calculated fluxes

The CO_2 flux measured by the LI-6262 in March was around 0.5 μmol m^{-2} s^{-1} with very little diurnal changes which is indicative of the ecosystem respiring CO_2. The LI-7200 produced very similar results for F_c and the mean difference relative to the LI-6262 was only -0.04 ± 0.32 μmol m^{-2} s^{-1} with an IQR of 0.62 μmol m^{-2} s^{-1} (Table 3). Though the IQR was on the order of the mean F_c it should be noted that the box plot of the LI-7200 – LI-6262 difference is centered on zero indicating little bias between these instruments (Fig. 8a). In contrast, the EC155 F_c had periods of negative F_c that were as large as -5 μmol m^{-2} s^{-1}, and the IRQ of difference relative to the LI-6262 was 1.36 μmol m^{-2} s^{-1}. The negative CO_2 flux values suggest that the forest ecosystem is absorbing CO_2 which is typically achieved by photosynthesis and is not ecologically likely for a senescent forest in mid-winter.

Latent heat flux was more episodic and all three IRGAs showed a similar trend (Fig. 8b). The mean LE from the LI-7200 and EC155 were both slightly larger than the LI-6262 (by 6 W m^{-2} for the LI-7200 and 4 W m^{-2} for the EC155) and there was fairly large variability in the differences (IQR for the LI-7200 – LI-6262 difference was 28.1 W m^{-2} while the EC155 – LI-6262 difference was 20.4 W m^{-2}, Table 3).

3.6 Comparison of spectra and ogives

Another way to examine the scalars and fluxes is to look at how the variance and flux change in the frequency domain. To achieve this, we created composite spectra and ogives (e.g., Friehe et al., 1991) where the data were selected based on daytime (Fig. 9a) and nighttime (Fig. 9b) periods. Because there are not large diurnal changes in F_c or LE during March, the results from the daytime and nighttime are similar, though stable, nocturnal conditions are typically more challenging for eddy-covariance instrumentation.

The vertical wind and sonic temperature spectra were similar for the three CSAT3's; however, there was less noise at high frequency in the CSAT3A data, presumably because the EC100 used a bandwidth filter set at 5 Hz. The CO_2 spectra from all three IRGAs shows mostly white noise (i.e., following a f^{+1} rise with increasing frequency) at frequencies larger than about 0.2 Hz (Kaimal and Gaynor, 1991). The LI-6262 CO_2 spectra also appear to contain extra variance in the frequency range of 0.002 to 0.1 Hz. Presumably, this was due to a combination of a weak CO_2 signal, long tubing, and (possibly) resonance from the rotary-vane pump increasing the variance in the measured CO_2. This extra variance does not appear to significantly affect the fluxes because the LI-6262 and LI-7200 F_c ogives are in good agreement which suggests that the extra LI-6262 CO_2 variance was not coupled with the vertical wind. The EC155 CO_2 spectra exhibit a strange peaked shape between about 0.1 and 1 Hz which appears to have a large effect on the resulting F_c ogives (suggesting that there was some correlation between this odd shape and the vertical wind). The reason for this odd spectral shape for EC155 CO_2 is currently unknown.

The specific humidity spectra from the three IRGAs

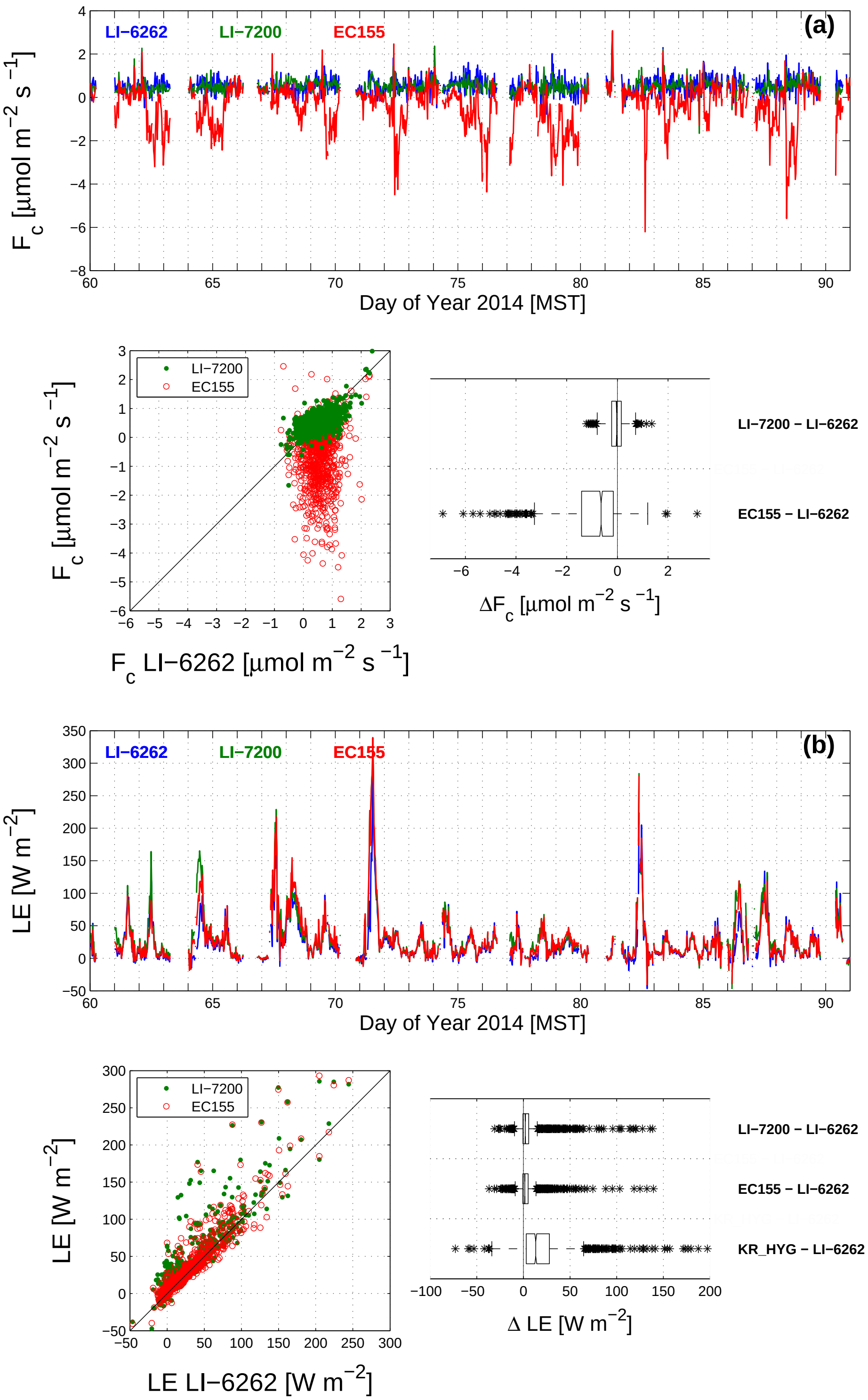

Figure 8: Time series, scatter plots, and box plots of the fluxes of (a) CO_2 F_c and (b) latent heat flux (LE) for the month of March, 2014. In the scatter plots, the fluxes from the LI-6262 is on the abscissa. In the box plots the differences relative to the LI-6262 fluxes are shown. In (b), the box plot includes the LE difference between the krypton hygrometer and LI-6262.

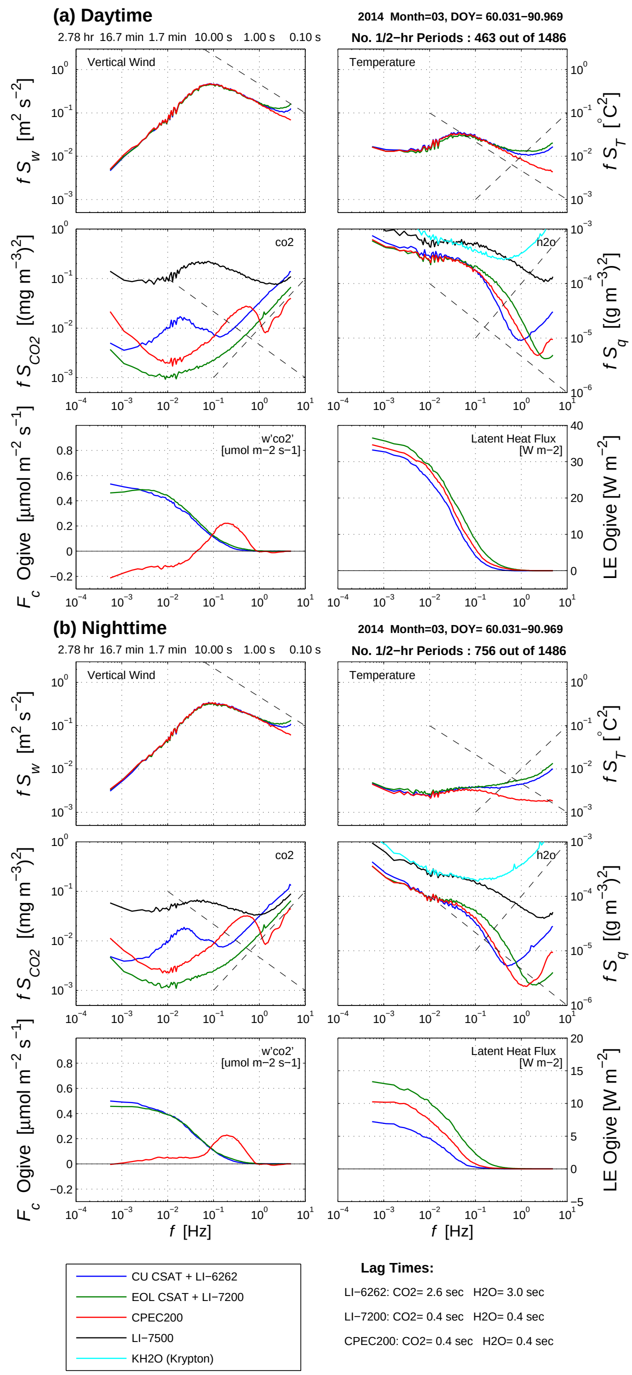

Figure 9: Median ensemble values of: vertical wind spectra S_w, sonic temperature spectra S_T, CO_2 spectra S_{CO_2}, specific humidity spectra S_q, and ogives of CO_2 flux F_c, and latent heat flux LE versus frequency f for **(a)** daytime and **(b)** nighttime periods. These are 30-min periods from March, 2014 with the number of periods in the ensemble listed above the S_T panel. In **(b)**, the legend and lag times shown apply to all panels. For S_{CO_2}, the CO_2 density ρ_c is used rather than χ_c (the conversion from μmol mol^{-1} to mg m^{-3} uses the molecular weight of CO_2 and the mean molar volume for each 30-min period). The dashed lines show a $f^{-2/3}$ and f^{+1} slope.

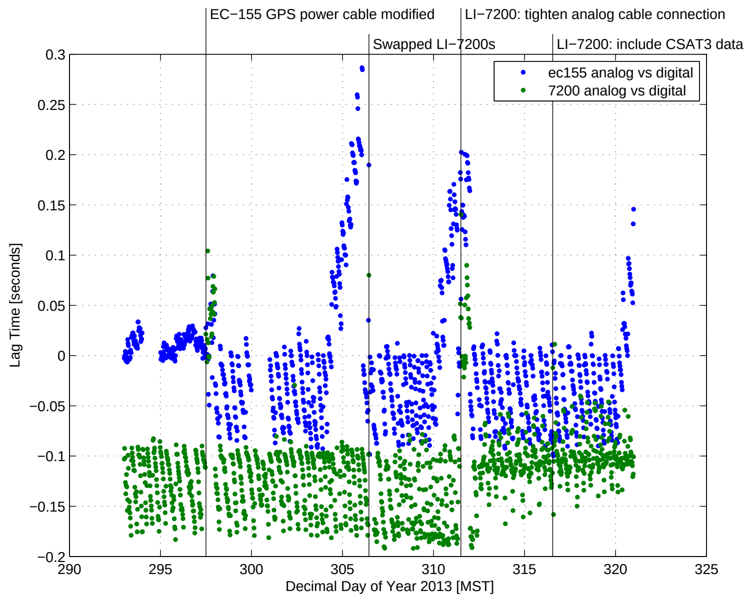

Figure 10: The lag time between the analog CO_2 dry mole fraction ingested by NIDAS versus the digital signal archived on the EC155 (blue symbols) and LI7200 (green symbols) IRGAs. A negative lag indicates that the digital signal precedes the analog signal in time. Events with the IRGAs are described by the vertical black lines and text above the figure.

agree well with each other up to a frequency of around 0.1 Hz (Fig. 9). At higher frequencies the LI-7200 stands out as having the largest variance/energy and does not start showing an effect of white noise until $f \approx 2$–3 Hz. In general, the white noise occurs at a slightly lower frequency during the nighttime periods than during the daytime (presumably due to the effects of stability on the atmospheric turbulence). The improved high-frequency response of the LI-7200 is likely due to a combination of: (1) the higher flow rate in the LI-7200, and (2) the heated intake tube which can extend the high-frequency range of an IRGA by several Hz (Metzger et al., 2014). In contrast, the LI-6262 shows the effects of white noise at $f \approx 0.8$–1 Hz and the EC155 at $f \approx 1$–2 Hz. Consistent with these responses to water vapor, the LI-7200 *LE* ogives have the largest flux, followed by the EC155 and the LI-6262. If we revisit the overall comparison of *LE* (i.e., Sect. 3.5, Table 3), the LI-7200 – LI-6262 mean *LE* difference was around 6 W m^{-2} whereas the EC155 – LI-6262 *LE* difference was around 4 W m^{-2}. Note that in March the average *LE* is on the order of 25 W m^{-2} so these mean differences are a significant percentage of the typical *LE*. Furthermore, the composite ogives shown in Fig. 9 suggest that these high-frequency differences in response led to the significant differences in the resulting *LE* flux.

In Fig. 9 we have included the spectra of the open-path LI-7500 (CO_2 and H_2O) and KH2O (H_2O). At the present time we only note that spectra from the open-path IRGAs have larger variance than those from the closed-path IRGAs due to the WPL effects on the air density discussed in Sect. 2.2.1.

3.7 Time-keeping comparisons

A comparison of the time lags (calculated from phase differences) between the analog CO_2 dry mole fraction ingested by NIDAS versus the digital CO_2 dry mole fraction on each of the IRGAs is shown in Fig. 10. The results show that the analog CO_2 output by the LI-7200 had a slight delay on the order 0.15 s) relative to the NIDAS system while those from the EC155 had a delay of 0.05 s. The 0.1 s range of the lags (shown by both IRGAs) was due to the slow drift in the CR23X data loggers used in the tower data system. An effort to remove this drift is currently being made.

4. DISCUSSION

One of the surprising results from our comparison is that F_c from the EC155 measured large negative fluxes during the month of March (Fig. 8a). In order to exam-

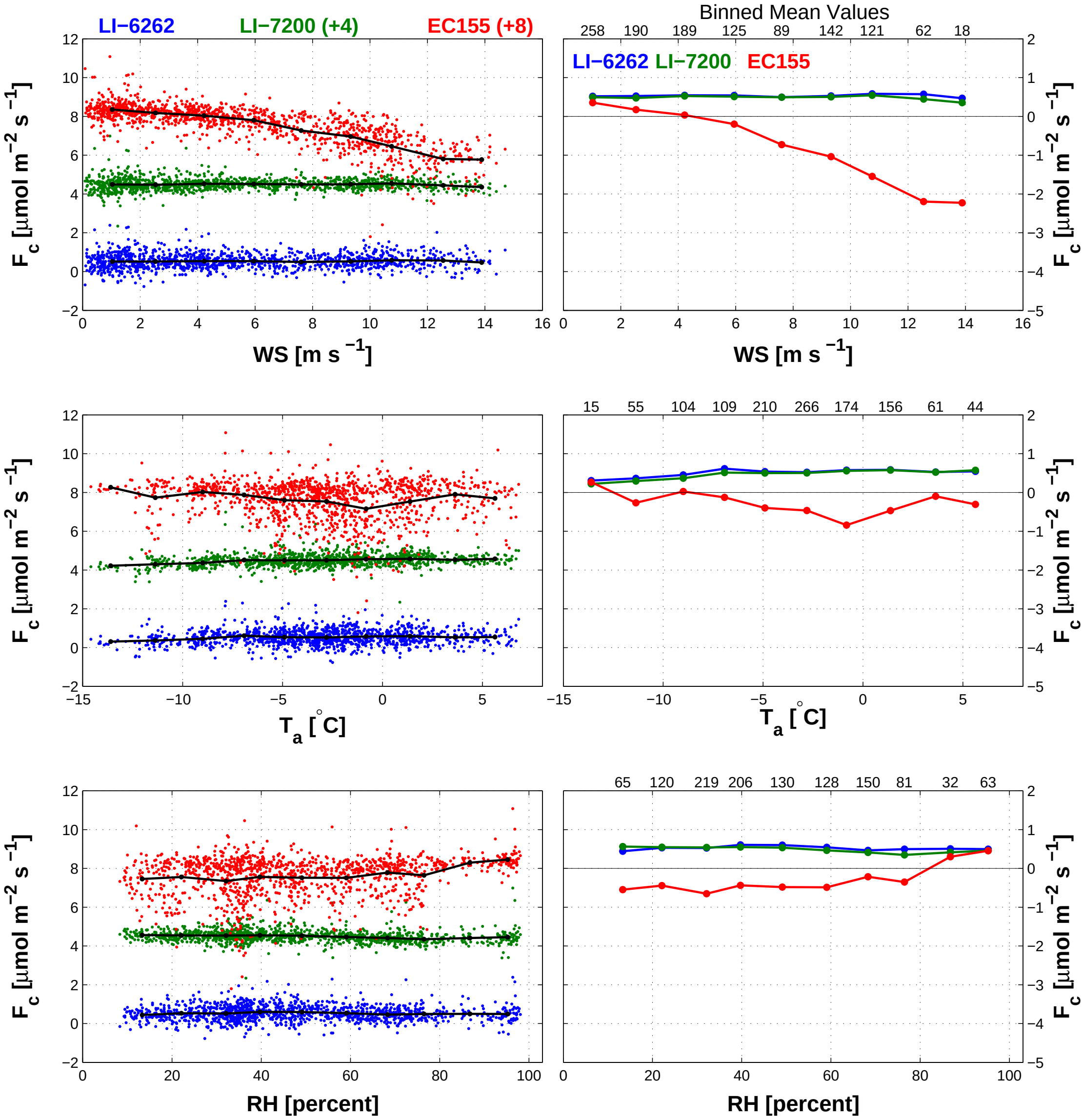

Figure 11: Turbulent vertical CO_2 fluxes F_c measured by the LI-6262, LI-7200, and EC155 versus the environmental variables of (top) wind speed WS, (middle) air temperature T_a, and (bottom) relative humidity RH. The left-hand panels show the 30-min values and the black line is the mean binned values. The data from the LI-7200 and EC155 are offset according to the text above the upper panel. The right-hand panel shows the mean binned values for each IRGA without any offset.

ine the reason for this behavior, we have plotted F_c for each IRGA versus the environmental variables of wind speed, air temperature, and relative humidity in Fig. 11. This plot reveals that the negative EC155 F_c were related to periods with high wind speeds. If we also examine the mean CO_2 in a similar way, and find that χ_c was not affected by wind speed in the same way (Fig. 12). In fact, none of these environmental variables could explain why χ_c displayed variations on the order of 15 μmol mol^{-1}.

One of the differences in instrument design between the LI-7200 and EC155 is how the cell temperature is measured. The LI-7200 uses two fast-response thermocouples to measure the temperature of the airstream as it enters and exits the sampling cell (e.g., Burba et al., 2010), whereas the CPEC200 uses a thermocouple embedded in the cell wall and is designed to remove any temperature fluctuations in the air sample so that the WPL temperature term in Eq.1 does not affect the flux measurements (Campbell Scientific, 2013b). Removal of air temperature fluctuations within a sampling tube is a well-known process (e.g., Leuning and Judd, 1996; Rannik et al., 1997; Sahlee and Drennan, 2009). It has been shown that a tubing length of 1000 times the tubing inner diameter will fully remove effects of temperature fluctuations on F_c though a significant percentage of the fluctuations are removed by shorter tubes (Rannik et al., 1997; Burba et al., 2010). Further evaluation of the temperature damping may be possible using the data collected during the IRGA comparison.

Considering the data problems with the EC155 CO_2,

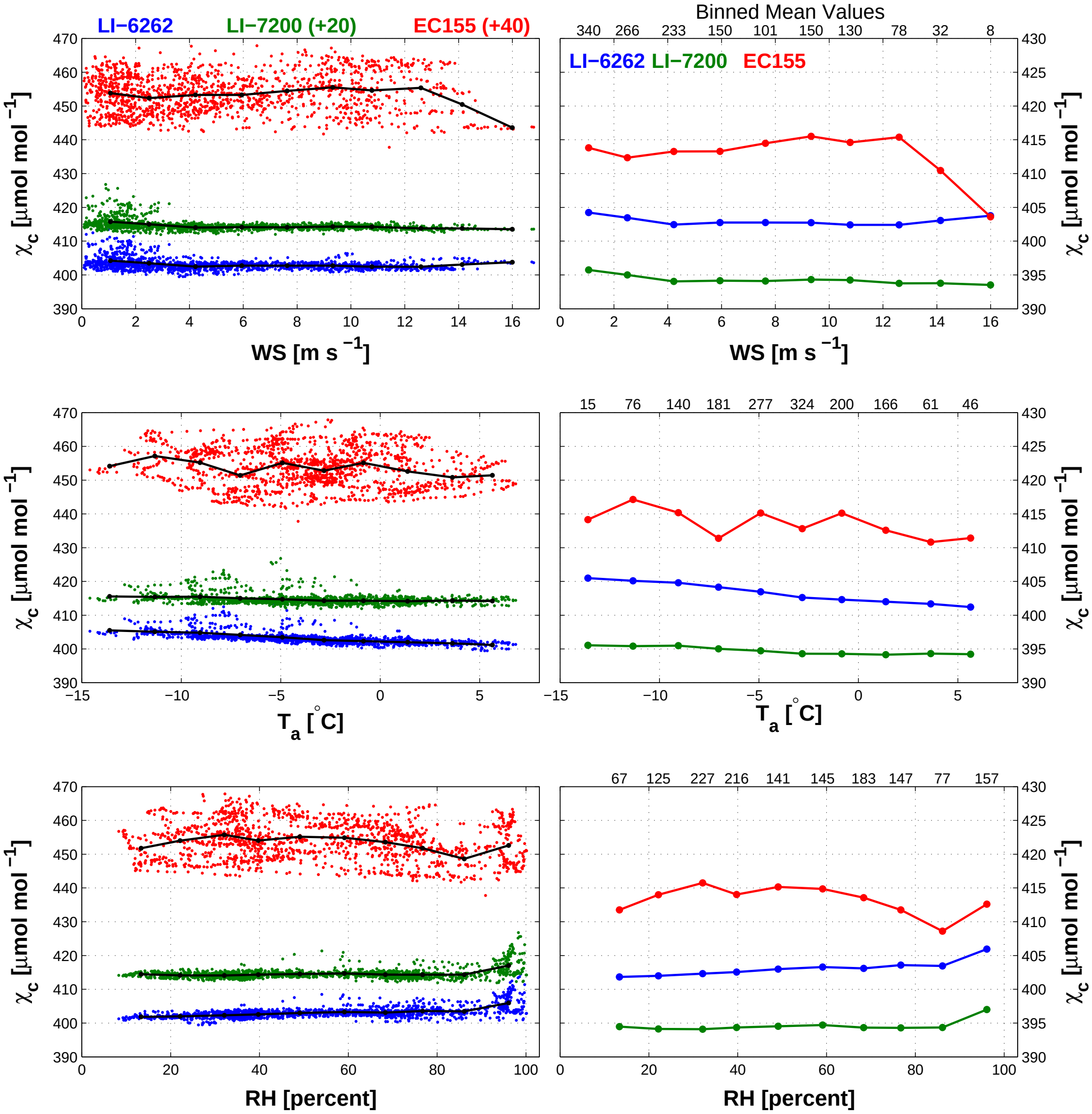

Figure 12: As in Fig. 11, except for CO_2 dry mole fraction χ_c.

we were unable to fully examine the differences in F_c between these two systems. Furthermore, the scale of the above-canopy turbulent transport of the scalars at this location might make it difficult to detect any high-frequency differences in the IRGAs. Such testing may be better suited in a region of higher turbulence such as a forest canopy or closer to the ground.

5. SUMMARY

A comparison of three IRGAs deployed above the forest at the Niwot Ridge AmeriFlux tower in March of 2014 was presented. Statistics from the comparison are summarized in Table 3 and our main findings are as follows:

- After applying the planar-fit, the statistics and vertical wind spectra from three side-by-side CSAT3's were fairly similar.
- Compared to the LI-6262, the LI-7200 had a 8.5 μmol mol^{-1} (2%) offset in mean CO_2, but F_c was similar. Spectral analysis revealed extra variance in the LI-6262 CO_2 in the frequency range of 0.002 to 0.1 Hz; however, ogive analysis of F_c showed little to no impact on the CO_2 flux.
- The EC155 measured large, unexplainable, variations in χ_c on the order of 15 μmol mol^{-1} (4%) that were not observed by any of the other CO_2 instruments. F_c and σ_{χ_c} from the EC155 exhibited an apparent wind speed dependence that resulted in unrealistic ecosystem fluxes of CO_2 in high winds.
- The estimated lag between the EC155 CO_2 and vertical wind resulted in the EC155 CO_2 fluctuations preceding those of the vertical wind. This is physically unlikely to occur on a regular basis. In contrast, the EC155 H_2O estimated time lags appeared reasonable.

- Based on water vapor spectra, the noise floor for H_2O during daytime was 3 Hz for the LI-7200, 2 Hz for the EC155, and 0.9 Hz for the LI-6262. The noise floor for the LI-7200 water vapor was improved by heating the incoming air (e.g., Metzger et al., 2014) which also appears to result in a higher latent heat flux. The noise floor for CO_2 spectra were less distinct.

- Consistent with the water vapor frequency response from each IRGA, the latent heat fluxes from the LI-6262 were smaller than the LI-7200 by around 6 $\mathrm{W\,m^{-2}}$ and smaller than the EC155 by around 4 $\mathrm{W\,m^{-2}}$. The ogives of *LE* suggest that these differences are due to differences in frequency response of each system, especially the long tubing used by the LI-6262.

The EC155 used in the IRGA comparison has been returned to Campbell Scientific for evaluation. Campbell Scientific will provide additional information to CPEC200 users as it becomes available.

The results shown here are preliminary. In order to complete the comparison, the humidity-dependence in the lag-time calculations as well as the decoupling of CO_2 and H_2O within the inlet tubing needs to be considered. Also, a more careful comparison to the open-path LI-7500 and KH2O sensor might provide additional insights not included here. Future possible analyses include: spectral coherence/phase differences between the sensors, closer examination of possible temperature fluctuations within the sample cell, and assessing the importance of using the lower-resolution analog CSAT3 winds ingested by the LI-7550 on the calculated fluxes. Finally, contrasting the cold-season IRGA comparison results presented here with those from the growing season will provide a more complete evaluation of the three IRGA sensors.

Acknowledgments: The AmeriFlux tower is supported by the AmeriFlux Management Project run by Lawrence Berkeley National Laboratory and has been supported by grants from the US Department of Energy (DOE), as well as NSF Long-Term Research in Environmental Biology (LTREB). Many scientists and engineers at the National Ecological Observatory Network (NEON), LI-COR, and Campbell Scientific have helped make this comparison possible. Xinhua Zhou provided helpful comments and Jason Hupp provided field support. Ted Hehn and Doug Kath from NEON helped with the LI-7200 heated inlet design. Dave Bowling (U. of Utah) kindly provided the TGA data. NCAR is sponsored by the National Science Foundation (NSF). NEON is a project solely funded by NSF and managed under a cooperative agreement by NEON, Inc. Any opinions, findings, and conclusions or recommendations expressed in this publication are those of the author(s) and do not necessarily reflect the views of NSF.

REFERENCES

Aubinet, M., T. Vesala, and D. Papale, 2012: *Eddy Covariance: A Practical Guide to Measurement and Data Analysis*, Springer Atmospheric Sciences, Dordrecht, The Netherlands, 438 pp.

Bowling, D. R., S. P. Burns, T. J. Conway, R. K. Monson, and J. W. C. White, 2005: Extensive observations of CO_2 carbon isotope content in and above a high-elevation subalpine forest, *Glob. Biogeochem. Cycle*, **19**, GB3023.

Bowling, D. R., W. J. Massman, S. M. Schaeffer, S. P. Burns, R. K. Monson, and M. W. Williams, 2009: Biological and physical influences on the carbon isotope content of CO_2 in a subalpine forest snowpack, Niwot Ridge, Colorado, *Biogoechemistry*, **95**, 37–59.

Burba, G., 2013: *Eddy Covariance Method for Scientific, Industrial, Agricultural, and Regulatory Applications: A Field Book on Measuring Ecosystem Gas Exchange and Areal Emission Rates*, LI-COR Biosciences, Lincoln, NE, USA, 331 pp.

Burba, G., A. Schmidt, R. L. Scott, T. Nakai, J. Kathilankal, G. Fratini, C. Hanson, B. Law, D. K. McDermitt, R. Eckles, M. Furtaw, and M. Velgersdyk, 2012: Calculating CO_2 and H_2O eddy covariance fluxes from an enclosed gas analyzer using an instantaneous mixing ratio, *Global Change Biology*, **18**, 385–399.

Burba, G. G., D. K. Mcdermitt, D. J. Anderson, M. D. Furtaw, and R. D. Eckles, 2010: Novel design of an enclosed CO_2/H_2O gas analyser for eddy covariance flux measurements, *Tellus Series B-Chemical And Physical Meteorology*, **62**, 743–748.

Burns, S. P., A. C. Delany, J. Sun, B. B. Stephens, S. P. Oncley, G. D. Maclean, S. R. Semmer, J. Schröter, and J. Ruppert, 2009: An evaluation of calibration techniques for in situ carbon dioxide measurements using a programmable portable trace-gas measuring system, *J. Atmos. Oceanic Technol.*, **26**, 291–316.

Burns, S. P., T. W. Horst, L. Jacobsen, P. D. Blanken, and R. K. Monson, 2012: Using sonic anemometer temperature to measure sensible heat flux in strong winds, *Atmos. Meas. Tech.*, **5**, 2095–2111.

Campbell Scientific, 2004: TGA100A Trace Gas Analyzer Overview, 14 pp., (Available at www.campbellsci.com).

—, 2010: CSAT3 Three Dimensional Sonic Anemometer Manual, Revision 6/10, 70 pp., (Available at www.campbellsci.com).

—, 2013a: CPEC200 Closed-Path Eddy-Covariance System Instruction Manual, Revision 12/13, 106 pp., (Available at www.campbellsci.com).

—, 2013b: EC155 CO_2 and H_2O Closed-Path Gas Analyzer Instruction Manual, Revision 5/13, 66 pp., (Available at www.campbellsci.com).

Clement, R. J., G. G. Burba, A. Grelle, D. J. Anderson, and J. B. Moncrieff, 2009: Improved trace gas flux estimation through IRGA sampling optimization, *Agric. For. Meteor.*, **149**, 623–638.

Devore, J. L., 1987: *Probability and Statistics for Engineering and the Sciences*, Brooks/Cole Publishing Company, Monterey, California, 672 pp.

Fratini, G., A. Ibrom, N. Arriga, G. Burba, and D. Papale, 2012: Relative humidity effects on water vapour fluxes measured with closed-path eddy-covariance systems with short sampling lines, *Agric. For. Meteor.*, **165**, 53–63.

Fratini, G., D. K. McDermitt, and D. Papale, 2014: Eddy-covariance flux errors due to biases in gas concentration measurements: origins, quantification and correction, *Biogeosciences*, **11**, 1037–1051.

Friehe, C. A., W. J. Shaw, D. P. Rogers, K. L. Davidson, W. G. Large, S. A. Stage, G. H. Crescenti, S. J. S. Khalsa, G. K. Greenhut, and F. Li, 1991: Air-sea fluxes and surface-layer turbulence around a sea-surface temperature front, *J. Geophys. Res.*, **96**, 8593–8609.

Fuehrer, P. L. and C. A. Friehe, 2002: Flux corrections revisited, *Bound.-Layer Meteor.*, **102**, 415–457.

Hoaglin, D. C., F. Mosteller, and J. W. Tukey, 1983: *Understanding Robust and Exploratory Data Analysis*, John Wiley & Sons, New York, 447 pp.

Hu, J., D. J. P. Moore, S. P. Burns, and R. K. Monson, 2010: Longer growing seasons lead to less carbon sequestration by a subalpine forest, *Global Change Biol.*, **16**, 771–783.

Ibrom, A., E. Dellwik, S. E. Larsen, and K. Pilegaard, 2007: On the use of the Webb-Pearman-Leuning theory for closed-path eddy correlation measurements, *Tellus Series B-Chemical And Physical Meteorology*, **59**, 937–946.

Kaimal, J. C. and J. E. Gaynor, 1991: Another look at sonic thermometry, *Bound.-Layer Meteor.*, **56**, 401–410.

Kowalski, A. S. and P. Serrano-Ortiz, 2007: On the relationship between the eddy covariance, the turbulent flux, and surface exchange for a trace gas such as CO_2, *Boundary-Layer Meteorology*, **124**, 129–141.

Lenschow, D. H. and M. R. Raupach, 1991: The attenuation of fluctuations in scalar concentrations through sampling tubes, *J. Geophys. Res.*, **96**, 15259–15268.

Leuning, R. and M. J. Judd, 1996: The relative merits of open- and closed-path analysers for measurement of eddy fluxes, *Global Change Biology*, **2**, 241–253.

LI-COR, 1996: LI-6262 CO_2/H_2O Analyzer Operating and Service Manual, Publication Number 9003-59, 3rd Printing, 120 pp., (Available at www.licor.com).

—, 2013: LI-7200 CO_2/H_2O Analyzer Instruction Manual, Publication Number 984-10564, 5th Printing, 194 pp., (Available at www.licor.com).

Maclean, G. and C. Webster, 2012: NCAR in-situ data acquisition software for airborne and surface measurements, in *16th Symposium on Meteorological Observation and Instrumentation*, New Orleans, LA. American Meteorological Society, 10.1, URL: https://ams.confex.com/ams/92Annual/webprogram/.

Massman, W. J., 1991: The attenuation of concentration fluctuations in turbulent-flow through a tube, *J. Geophys. Res.*, **96**, 15269–15273.

Mauder, M., T. Foken, R. Clement, J. A. Elbers, W. Eugster, T. Grunwald, B. Heusinkveld, and O. Kolle, 2008: Quality control of CarboEurope flux data - Part 2: Inter-comparison of eddy-covariance software, *Biogeosciences*, **5**, 451–462.

McDermitt, D. K., 1997: *Some recommendations for using LI-COR Gas Analyzers in Eddy Correlation Measurements. Topics discussed at Ameriflux Workshop, 1996*, Application Note #118, LI-COR Inc., Lincoln, Nebraska, 7pp., (Available at www.licor.com).

Metzger, S., S. Burns, H. Luo, T. Hehn, D. Kath, G. Burba, J. Li, T. Anderson, P. D. Blanken, and J. Taylor, 2014: A gas analyzer sampling system optimized for eddy-covariance applications, in *17th Symposium on Meteorological Observation and Instrumentation*, Westminister, CO. American Meteorological Society, 3, URL: https://ams.confex.com/ams/21Applied17SMOI/.

Monson, R. K., S. P. Burns, M. W. Williams, A. C. Delany, M. Weintraub, and D. A. Lipson, 2006: The contribution of beneath-snow soil respiration to total ecosystem respiration in a high-elevation, subalpine forest, *Glob. Biogeochem. Cycles*, **20**, GB3030.

Monson, R. K., M. R. Prater, J. Hu, S. P. Burns, J. P. Sparks, K. L. Sparks, and L. E. Scott-Denton, 2010: Tree species effects on ecosystem water-use efficiency in a high-elevation, subalpine forest, *Oecologia*, **162**, 491–504.

Monson, R. K., A. A. Turnipseed, J. P. Sparks, P. C. Harley, L. E. Scott-Denton, K. Sparks, and T. E. Huxman, 2002: Carbon sequestration in a high-elevation, subalpine forest, *Global Change Biol.*, **8**, 459–478.

Nakai, T., H. Iwata, and Y. Harazono, 2011: Importance of mixing ratio for a long-term CO_2 flux measurement with a closed-path system, *Tellus Series B-Chemical And Physical Meteorology*, **63**, 302–308.

Novick, K. A., J. Walker, W. S. Chan, A. Schmidt, C. Sobek, and J. M. Vose, 2013: Eddy covariance measurements with a new fast-response, enclosed-path analyzer: Spectral characteristics and cross-system comparisons, *Agric. For. Meteor.*, **181**, 17–32.

Rannik, U., T. Vesala, and R. Keskinen, 1997: On the damping of temperature fluctuations in a circular tube relevant to the eddy covariance measurement technique, *J. Geophys. Res.*, **102**, 12789–12794.

Sahlee, E. and W. M. Drennan, 2009: Measurements of damping of temperature fluctuations in a tube, *Bound.-Layer Meteor.*, **132**, 339–348.

Sargent, S., 2012: Quantifying frequency response of a low-power, closed-path CO_2 and H_2O eddy-covariance system, 10 pp., (Available at www.campbellsci.com).

Schaeffer, S. M., J. B. Miller, B. H. Vaughn, J. W. C. White, and D. R. Bowling, 2008: Long-term field performance of a tunable diode laser absorption spectrometer for analysis of carbon isotopes of CO_2 in forest air, *Atmospheric Chemistry And Physics*, **8**, 5263–5277.

Scott-Denton, L. E., K. L. Sparks, and R. K. Monson, 2003: Spatial and temporal controls of soil respiration rate in a high-elevation, subalpine forest, *Soil Biology & Biochemistry*, **35**, 525–534.

Trivett, N. and A. Köhler, 1999: Guide on sampling and analysis techniques for chemical constituents and physical properties in air and precipitation as applied at stations of the Global Atmosphere Watch. Part I: Carbon dioxide, Technical report, WMO Tech. Doc. No. 980; Global Atmosphere Watch (GAW) Report No. 134.

Turnipseed, A. A., P. D. Blanken, D. E. Anderson, and R. K. Monson, 2002: Energy budget above a high-elevation subalpine forest in complex topography, *Agric. For. Meteor.*, **110**, 177–201.

Webb, E. K., G. I. Pearman, and R. Leuning, 1980: Correction of flux measurements for density effects due to heat and water-vapor transfer, *Quarterly Journal Of The Royal Meteorological Society*, **106**, 85–100.

Welles, J. M. and D. K. McDermitt, 2005: Measuring carbon dioxide in the atmosphere, in *Micrometeorology in Agricultural Systems*, pp. 287–320, (Available at www.licor.com).

Wilczak, J. M., S. P. Oncley, and S. A. Stage, 2001: Sonic anemometer tilt correction algorithms, *Bound.-Layer Meteor.*, **99**, 127–150.

Zhao, C. and P. P. Tans, 2006: Estimating uncertainty of the WMO mole fraction scale for carbon dioxide in air, *J. Geophys. Res.*, **111**, D08S09.